REPORT DOCUMENTATION PAGE

Form Approved
OMB NO. 0704-0188

1. AGENCY USE ONLY (Leave Blank)	2. REPORT DATE	3. REPORT TYPE AND DATES COVERED Reprint

4. TITLE AND SUBTITLE
Materials Science Aspects of Weld Corrosionl

5. FUNDING NUMBERS
DAAD19-01-1-0375

6. AUTHOR(S)
See attached report

7. PERFORMING ORGANIZATION NAME(S) AND ADDRESS(ES)
Colorado School of Mines
1500 Illinois St.
Golden CO 80401-1890

8. PERFORMING ORGANIZATION REPORT NUMBER

9. SPONSORING / MONITORING AGENCY NAME(S) AND ADDRESS(ES)
U. S. Army Research Office
P.O. Box 12211
Research Triangle Park, NC 27709-2211

10. SPONSORING / MONITORING AGENCY REPORT NUMBER
41923.18-MS

11. SUPPLEMENTARY NOTES
The views, opinions and/or findings contained in this report are those of the author(s) and should not be construed as an official Department of the Army position, policy or decision, unless so designated by other documentation.

12 a. DISTRIBUTION / AVAILABILITY STATEMENT
Approved for public release; distribution unlimited.

13. ABSTRACT (Maximum 200 words)
See Attached Report

14. SUBJECT TERMS			15. NUMBER OF PAGES 16. PRICE CODE
17. SECURITY CLASSIFICATION OR REPORT **UNCLASSIFIED**	18. SECURITY CLASSIFICATION ON THIS PAGE **UNCLASSIFIED**	19. SECURITY CLASSIFICATION OF ABSTRACT **UNCLASSIFIED**	20. LIMITATION OF ABSTRACT **UL**

Proc. Of International Conference on Welding and Joining of Materials, Pontifica Universidad Catolica del Peru, October 27-29, 2003, Lima, Peru (2003)

Materials Science Aspects of Weld Corrosion

D.L. Olson, A.N. Lasseigne, M. Marya, B. Mishra and G.Castro

Center for Welding, Joining and Coatings Research
The G.S. Ansell Department of Metallurgical and Materials Engineering
Colorado School of Mines, Golden CO 80401 (USA)

ABSTRACT - Corrosion is an environmentally assisted damage that professionals face daily, particularly with welded structures. Fusion welds result from solidification and solid-state transformations induced by well-localized thermal cycles. A fusion weld joint inherently exhibits an irregular surface as well as gradients in chemical composition, microstructure, properties and residual stress, depending upon process parameters and part geometry. This article analyzes the roles of surface topography, alloy chemical compositional variation, hydrogen distribution, and stress on weld corrosion.

1. INTRODUCTION

Corrosion is a natural process resulting from the inherent tendency of metals to revert to their most stable form, usually oxides and hydroxides. Weldments are associated with many types of corrosion, but are particularly susceptible to chemical dissolution, galvanic and pitting corrosion, stress-corrosion cracking and hydrogen assisted cracking.

Chemical dissolution is a type of corrosion that occurs when a metal is anodically attacked and reduced to ions. Chemical dissolution is discussed in Section 2, and the role of surface topography is analyzed with respect to this type of corrosion in Section 3. Pitting corrosion behavior is addressed in Section 4. Galvanic corrosion is an electrochemical process occurring between two different metallic contacted components with an electrolyte acting as a charge transport medium. The ionicity of the electrolyte guarantees a columbic exchange between at least two metallic phases of unlike chemical potential, where one acts as an electron consumer and the other a cation donor. Because metallic phases can each be characterized by a specific chemical potential, a dissimilar metal weldment is always a subject of galvanic corrosion when a fluid and electrical junction is established between the constituents, either permanently or temporarily. In welds with compositionally non-uniform characteristics, galvanic attack can occur at the microstructural level. Galvanic corrosion is analyzed in Section 5 and stress corrosion is Section 6. New approaches in hydrogen management in steel welds are introduced in Section 7 and a microbiologically influenced corrosion on welds is described in Section 8.

In fusion welding, the temperatures vary rapidly within the assembly, depending upon the alloy thermo-physical properties and the welding parameters. In the melt, temperatures approach the material melting temperature near the weld interface (Figure 1) and may exceed the boiling temperature at the pool center. Cooling rates may be as low as 10^{2}°C/s in conventional arc welding and as high as 10^{6}°C/s in high power density welding.

Depending upon alloy systems and joining processes, a weldment typically consists of five microstructurally distinct regions, normally identified as the fusion zone, the unmixed region (part of the fusion zone), the partially melted region (part of the heat-affected zone), the heat-affected zone, and the base metal, as illustrated in Figure 1.

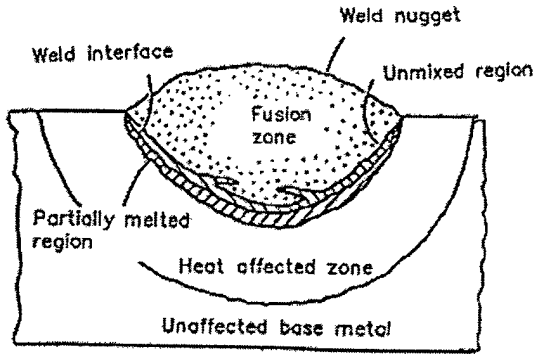

Figure 1: Heterogeneous regions of a fusion weld [1].

The fusion zone is frequently the result of melting between two identical base metals and a filler metal of a different chemical composition. When its chemical composition differs from that of the base metal, a macroscopic galvanic couple forms and influences the corrosion process near the weld. On a finer scale, the fusion zone is also characterized by micro-galvanic cells, which are mainly created from partitioning of the alloying elements during cooling, resulting from microstructural solute segregation during rapid solidification [2].

When detectable, the thin unmixed region is also subject to corrosion caused by the melting and solidification of the base metal into a composition similar to the base metal. When Type 304-stainless steel is fusion welded using high chromium-nickel filler metal, steep concentration gradients of chromium and nickel are established in the fusion zone, whereas the unmixed zone exhibits a composition comparable to the base metal. Corrosion susceptibility of steel is increased due to reduced chromium concentrations or chromium passivation at the surface.

Sputtered neutral mass spectroscopy also reveals evidence of spatial elemental variations in an oxide layer composition in the depth direction of the heat-affected zone, as shown in Figure 2. Iron is enriched in the outermost oxide region, and chromium is enriched in the layers beneath. The iron rich oxide suddenly

disappears at a given position in the HAZ, beyond which pure chromium oxide is observed. This compositional variation in the passive oxide over the heat-affected zone supports the evidence that the HAZ region near the fusion line is often the position of corrosion attack.

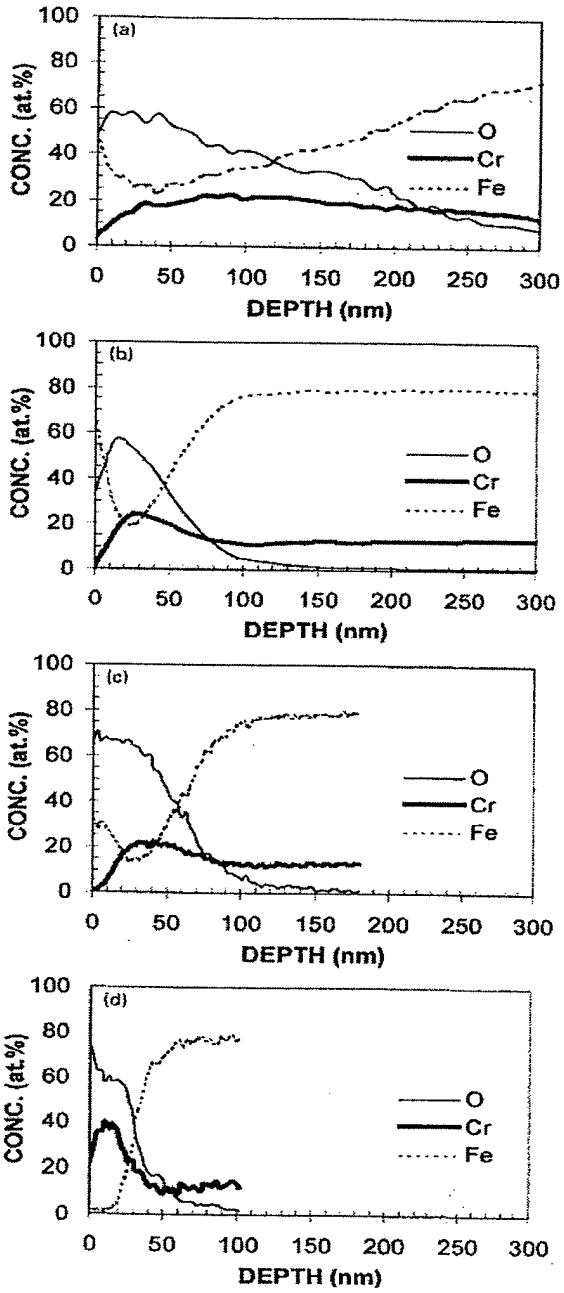

Figure 2: Measured oxide layers at varying depths across the heat-affected zone of a stainless steel weld (a) 1 mm from fusion line, (b) 4.5 mm from fusion line, (c) 6 mm from fusion line, (d) 7 mm from fusion line [3].

The heat-affected zone experiences lower peak temperatures when compared to the fusion zone, but still experiences high cooling rates. Because each position of the heat-affected zone has its own unique time-temperature cycle, microstructural gradients also exist within the heat-affected zone. Microstructural gradients can lead to intergranular corrosion caused by chromium depletion due to carbide precipitation along grain boundaries, as detailed in Section 5. Comparable gradients are also encountered within solidified multi-pass welds due to bead-to-bead variations in degree of solute mixing and thermal experience.

Between the fusion zone and the heat-affected zone exists a tiny region called the partially melted region, usually spread over one or two grains. Although restricted, grain boundary liquation followed by cracking is a common difficulty in both aluminum alloys and superalloys. Cracks along grain boundaries over a distance as small as a grain have been identified as potential initiation sites for hydrogen-promoted underbead cracking in high-strength steel.

Gradients on a similar scale exist within solidified multi-pass weld metal due to bead-to-bead variations in thermal experience. Compositional gradients on the scale of a few microns, referred to as microsegregation, exist within individual grains in weld beads due to segregation of major and trace elements during solidification.

Welding parameters determine the morphology and scale of fusion zone microstructures, the extent of other metallurgical zones, the degree of segregation (compositional heterogeneity), the distribution of inclusions, and the presence of defects such as hot cracks; the welding process also leaves residual stresses resulting from the thermal experiences. Furthermore, the surface of a weld typically exhibits ripples, as shown in Figure 3, where localized corrosion may develop due to compositional gradients and surface curvature.

All of these factors affect the weldment resistance in a chemically aggressive environment. These factors are discussed using thermodynamic, electrochemical and mechanical fundamentals.

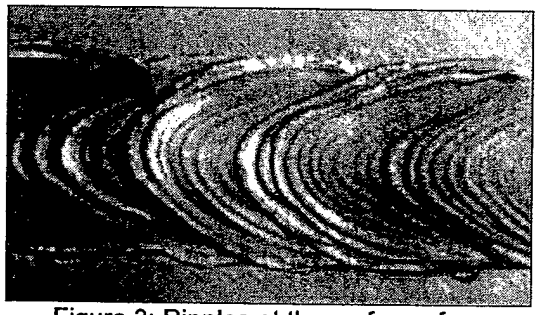

Figure 3: Ripples at the surface of an autogeneous laser weld.

2. CHEMICAL DISSOLUTION (UNIFORM CORROSION)

In many situations, corrosion is observed to develop quite uniformly over a metal surface. The rate at which the metal is chemically attacked or passivated (when a adhesive and protective layer is formed) depends upon the mechanistic mobility and the chemical driving energy at the metal/solution interface, expressed as either the free energy for the reaction of metal dissolution, or the chemical potential of the metal M, μ_M, in both the metal and the solution. As a result, metal loss can be linear, parabolic, exponential, logarithmic, or a combination of various scale laws depending upon the time variation for specific metal removal or atomic transport mechanisms. Figure 4 depicts a case in which the metal M is uniformly dissolved into cation M^{n+}

(where n is the valence). The volumetric free energy that corresponds to the dissolution of the metal M can be detailed by the following half-cell reactions:

$$M \rightarrow M^{n+} + ne^- \quad (1)$$

$$ne^- + nH^+ \rightarrow \frac{n}{2} H_2 \quad (2)$$

corresponding to the overall dissolution reaction:

$$M + nH^+ \rightarrow M^{n+} + \frac{n}{2} H_2 \quad (3)$$

The free energy change for Eq. 3 can therefore be expressed as:

$$\Delta G = \Delta G_0 + RT \ln \frac{\left[M^{n+}\right]}{\left[H^+\right]^n} \quad (4)$$

assuming that solutions are Raoultian, the metal is pure and the hydrogen generation produces bubbles (P_{H2}=1 atm).

Correspondingly, this free energy difference can also be determined from the M/M^{n+} potential with respect to normal hydrogen potential (H^+/H_2):

$$\Delta G = -nF\left(E_{M+/M} - E_{H+/H_2}\right) \quad (5)$$

These potentials can be determined by using the Nernst equation for the environmental conditions of interest. The damage will be a uniform dissolution of a flat surface resulting in a uniform wastage or thinning of an alloy plate.

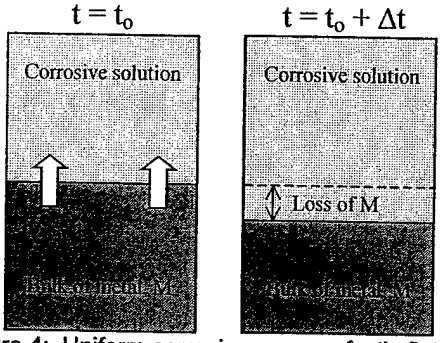

Figure 4: Uniform corrosion on a perfectly flat and chemically homogenous surface.

3. EFFECT OF SURFACE TOPOGRAPHY

While uniform corrosion often applies to a macroscopic scale, as-fabricated surfaces and weld surfaces are inherently rough, thereby exhibiting discontinuities and chemical potential gradients due to surface curvature. Although the chemical driving energy, ΔG, can be very large, particularly for the reactive and light metals, a contribution from the surface curvature may also be anticipated.

Figure 3 shows the formation of ripples at the surface of an autogeneous solute-lean magnesium laser weld due to temperature gradients and surface tension driven flow in the solidifying melt. These ripples (on a macroscopic level) as well as micro-asperities (on the microscopic level) are geometrical imperfections that locally influence the free energy of the surface and the chemical potential of an atom of M on this surface.

The atoms at the surface of micro-asperities are treated differently than the atoms on a flat surface. The effect of surface curvature (capillarity) on the chemical potential is well described by the Gibbs-Thomson equation, expressed as:

$$\mu = \mu_0 \pm C \frac{\Omega \gamma}{r} \quad (6)$$

where μ is the chemical potential, μ_0 is the chemical potential of an atom on a flat surface, C is a capillarity constant (1 for a cylindrical surface, 2 for a spherical surface), Ω is the atomic volume, γ is the surface tension, and r is the radius of curvature. Eq. 6 demonstrates that chemical potential is maximized for a small positive radius of curvature. Introduction of numerical data into Eq. 6 also shows that curvature affects chemical potential when radius of curvature reaches the sub micron level.

To discuss the contribution of surface micro-asperities on corrosion, a periodic surface topography of wavelength 4r with maximum height 2r and half-cylindrical surface of radius r, as shown in Figure 5, is assumed. At any location under the average surface, radius of curvature r has a negative value and thus decreases the chemical potential by the Gibbs-Thomson parameter (γΩ/r). At mid-point (i.e. on the average surface), the chemical potential reduces to μ_0. On the region above the average surface height, the chemical potential is increased by the constant amount, γΩ/r. Because chemical potential is highest above the average surface, dissolution of the metal M will be faster at the top than at the bottom of the surface. As dissolution proceeds and assuming no changes in the corrosive solution, the surface will gradually flatten until the chemical potential becomes equal across the surface. Dissolution of the metal then proceeds at a constant rate isotropically.

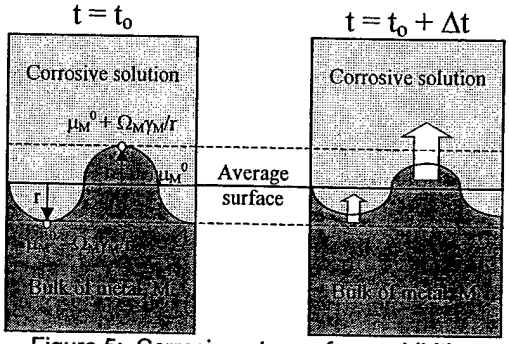

Figure 5: Corrosion at a surface exhibiting small radii of curvature.

4. PITTING CORROSION: A NUCLEATION AND GROWTH EVENT

Pitting corrosion is defined as an accelerated form of chemical attack in which the rate of corrosion is greater in some localized areas than others. Pitting is often a localized attack caused by a breakdown in the thin passive oxide film that protects material from the corrosion process. Pit growth normally is driven by a concentration cell established due to a

compositional gradient of the solution that is in contact with the alloy material. Such compositional gradients result when the solution at a surface irregularity is different from that of the bulk solution concentration. In stainless steels, pitting often occurs when the corrosive environment penetrates the passivated film in only a few areas, as opposed to the overall surface.

Because surface energy must affect pit formation, pitting corrosion can be treated as a nucleation and growth process, where surface energy promotes an activation barrier. The situation where a pit acts as a nucleation site for further dissolution of the metal M is addressed in the next developments.

The concentration, N (number of pits per area), of critical-sized pits, which relates to their nucleation rate, is assessed to be thermally activated and given by a Boltzmann distribution as:

$$N^* = N_0 \cdot \exp\left(\frac{-\Delta G^*}{kT}\right) \tag{7}$$

where ΔG^* is the free energy barrier that must be overcome for pit formation and thus pitting corrosion to proceed, k is the Boltzmann constant, and T is the absolute temperature.

The nucleation of a semi-spherical pit on a microscopically flat surface of radius r, as shown in Figure 6, can be described as a free energy change, having a volume and surface contribution. Volume free energy includes a negative energy component, ΔG_v, which corresponds to the reaction in Eq. 3 and is given by Eq. 4. Contributions due to lattice defect reductions and residual strains are also assumed to be included in ΔG_V. The creation of a surface, as shown in Figure 5, necessitates extra energy for the creation of the extra surface area of the pit, which opposes the volumetric free energy reduction. With all these contributions, the total free energy change, $\Delta G_{1\to 2}$ from State 1 to State 2, without taking into consideration curvature, can be expressed as:

$$\Delta G_{1\to 2} = (\Delta G_v)\big|_{\pi 0}\left(\frac{2}{3}\pi r^3\right) + \gamma_m (2\pi r^2)\big|_{\phi 0} \tag{8}$$

The barrier to nucleation has a maximum free energy change (ΔG^*), and can be determined when the following condition is satisfied:

$$\left.\frac{d\Delta G_{1\to 2}}{dr}\right|_{r=r^*} = 0 \tag{9}$$

where r* is the critical radius to nucleation. Derivation shows that:

$$r^* = -\frac{2\gamma_M}{\Delta G_v\big|_{<0}} \tag{10}$$

and:

$$\Delta G^* = -\frac{16\pi\gamma_M^3}{3\left(\Delta G_v\big|_{<0}\right)^2} \tag{11}$$

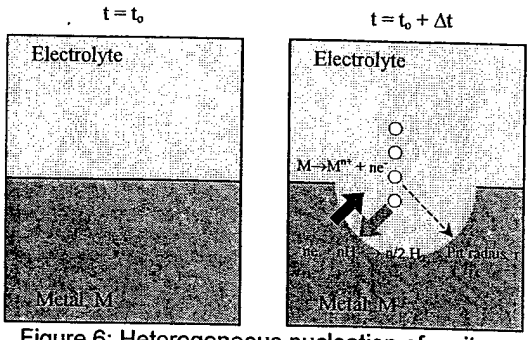

Figure 6: Heterogeneous nucleation of a pit on a pure metal with a perfectly flat surface.

Eq. 10 shows that the critical pit radius will be small when the chemical free energy change is large, as is confirmed in Figure 7 with actual data for a number of elements. Because the driving force for the dissolution of the metal is exceedingly large (Eq. 4), the critical radii for pit nucleation in metals (Figure 7) reach values that are lower than atomic radii. This simple calculation implies that corrosion will proceed regardless of the topography. For an initially perfectly flat surface, spontaneous pit formation is therefore not possible because uniform corrosion will occur across the surface.

In real situations, however, pitting is observed even on high purity metals. The presence of pits in the exposed metal suggests that any local perturbation in the electrolyte, particularly in its chemical composition, must play a dominant role.

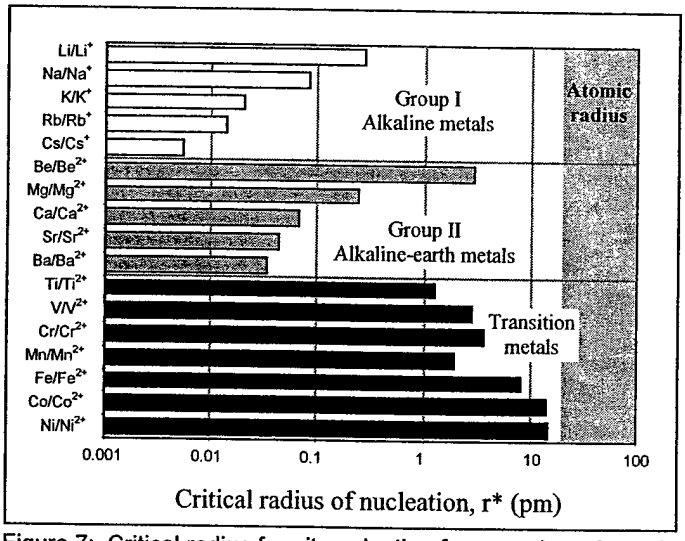

Figure 7: Critical radius for pit nucleation for a number of metals.

As stated earlier, for an initially perfectly flat surface, pitting is not possible because uniform corrosion will occur across the surface. However, if the same macroscopically flat surface in Figure 6 has a passive layer, the corrosion may no longer be uniform across the surface. If the passive layer cracks, then that area is more susceptible to corrosion than other areas of the metal surface. This type of behavior is most likely to occur in the heat-affected zone, which is more sensitized to corrosion due to composition and thickness variations of the passive films in the heat-affected zones (Figure 2).

The effect of composition on a cell potential can be described through the Nernst equation, where anodic and cathodic sites are characterized by different potentials due to chemical composition variations in the alloy and/or electrolyte.

Using the concept of cell potentials, a critical cell potential must be overcome for a perfectly flat surface of a pure metal to form a pit. In the close vicinity of an interface, it may be hypothesized that there are fluctuations in the chemical potential, either due to variations in temperature or local composition, as promoted by lack of fluid flow. This change in potential generates a concentration cell, and it can be hypothesized that this difference in potential promotes pit growth, as shown in Figure 8.

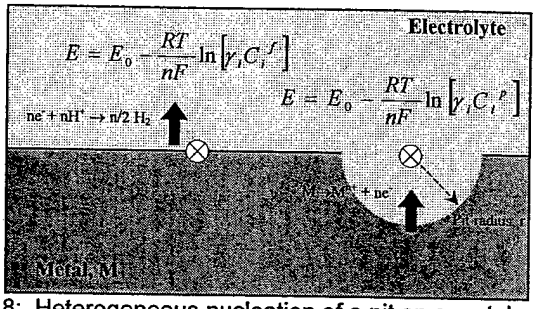

Figure 8: Heterogeneous nucleation of a pit on a metal surface.

The above discussion can describe pit growth, but the actual nucleation of the pit will have to include the overcoming of the nucleation energy barrier that has both surface energy contribution due to pit surface area and pit curvature contribution due to the Gibbs-Thomson expression. The total free energy, including the Gibbs-Thomson effect, is now given for a semi-spherical pit as:

$$\Delta G_{1-2} = (\Delta G_v) * (\tfrac{2}{3}\pi r^3) + \frac{2\Omega\gamma}{r}(\frac{2\pi r^3}{3\Omega}) + 2\gamma\pi r^2 \quad (12)$$

Differentiating Eq. 12 with respect to r, the critical radius r* becomes:

$$r^* = \frac{-(10/3)\gamma}{\left(-B\ln\left[\frac{M^{++}}{M^{++}}\right]_C\right)} \quad (13)$$

where the term $(-B*\ln([M^{++}]_C/[M^{++}]_F)$ is the chemical potential difference expressed as a ratio of the concentration of metal ions with a curved surface over the concentration of metal ions with a flat surface in which -B is a function of n, Faraday constant, F, and RT.

Figure 9 shows the relationship of the critical radius as a function of the ratio of concentration of metal ions on a curved surface over the concentration of metal ions on a flat surface. When the localized solute atoms become more concentrated, the critical radius at such location gets smaller, making pit growth easier to attain. Whereas the localized solute atoms become less concentrated, the critical radius goes toward infinity, making pit nucleation significantly more difficult.

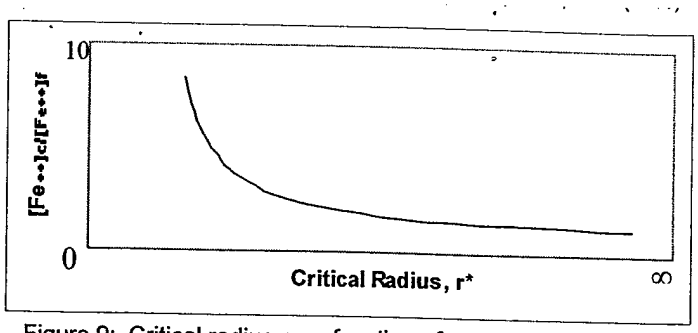

Figure 9: Critical radius as a function of concentration ratio.

5. GALVANIC CORROSION IN WELDMENTS

Welding thermal cycles tend to promote heterogeneous microstructures, i.e., galvanic cells. The use of filler metals with compositions different from the base material yield electrochemical potential differences, thus making regions of weldments more active. For a majority of aluminum alloys, the weld metal and the heat-affected zone become more noble relative to the base metal, as demonstrated in Figure 10 (a) and (b) for a saltwater environment. Certain aluminum alloys form narrow anodic regions in the heat-affected zone and are prone to localized attack. Alloys 7005 and 7039 are particularly susceptible to this problem (Figure 10c) [1].

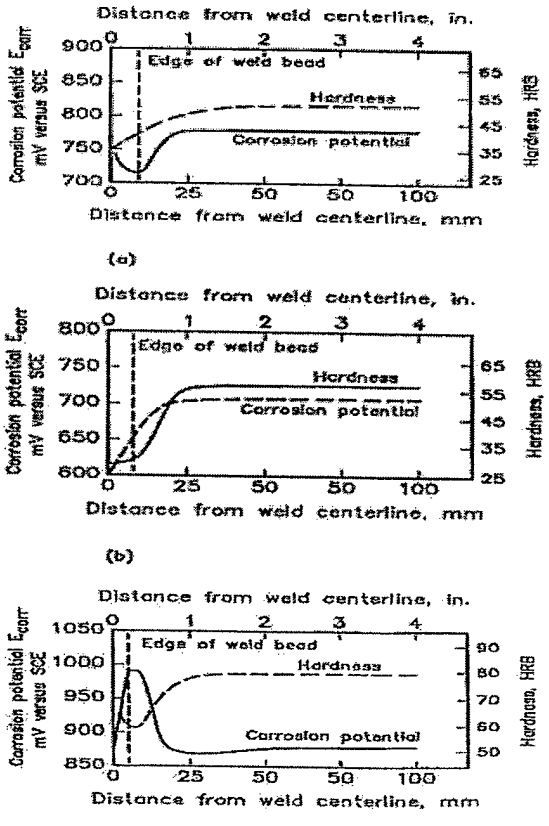

Figure 10: Effect of welding heat on microstructure, hardness, corrosion potential of three aluminum alloy welded assemblies. (a) Alloy 5456-H321 base metal with alloy 5556 filler. (b) Alloy 2219-T87 base metal with alloy 2319 filler. (c) Alloy 7039-T651 base metal with alloy 5183 filler. [1]

In the vicinity of an electrochemically inert precipitate, the composition of the solid solution changes locally. Solute concentrations can be either increased or decreased, depending on what is depleted due to formation of the new phase.

The microstructure of a two-phase alloy, α(A-atom rich phase) and β(B-atom rich phase), is unstable if the interfacial energy is not minimal. Therefore, given time and enough thermal energy, a high density of small particles will tend to coarsen into a larger particle (Ostwald ripening) [4]. During this process, the solubility of the α-phase for the B atoms of the β phase will increase, causing the α phase to be sensitive to the size of the β-phase particles. In localized precipitation hardening alloys (Type 2xxx, 6xxx, 7xxx aluminum alloys), overaging exhibits this localized change in solute adjacent to the particle, resulting in susceptibility to localized galvanic attack.

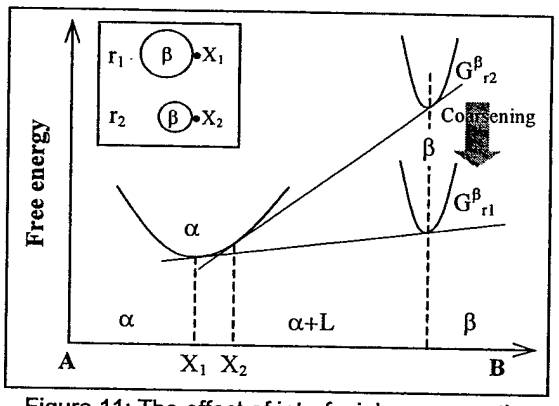

Figure 11: The effect of interfacial energy on the solubility near small particles [4].

In Figure 11, consider two adjacent spherical precipitates with different diameters and concentrations r_1, X_1 and r_2, X_2. Due to the Gibbs-Thomson effect, the solute concentration in the matrix adjacent to the particle will increase as the radius of curvature decreases, causing concentration gradients and a tendency for localized galvanic attack. As the particle radius increases, the solute level becomes less concentrated, so the susceptibility for localized galvanic attack decreases [4]. It is common to use certain aluminum alloys in a slightly over-aged condition to improve the corrosion resistance. For example, over-aging has been used to retard stress corrosion cracking in high strength aluminum alloys.

Weld Decay of Stainless Steel

During welding of stainless steels, locally sensitized regions (i.e., regions susceptible to corrosion) often develop. Sensitization is due to the formation of chromium carbide along grain boundaries, resulting in depletion of chromium in the region adjacent to the grain boundary. Chromium depletion produces localized galvanic cells, as shown in Figure 12. If this depletion drops the chromium content below the necessary 12 wt. pct., the chromium content that is required to maintain a protective passive film, the region will become susceptible to corrosion, resulting in intergranular attack. This type of corrosion most often occurs in the heat-affected zone. Intergranular corrosion causes a loss of metal in a region that parallels the weld deposit. This corrosion behavior is called weld decay.

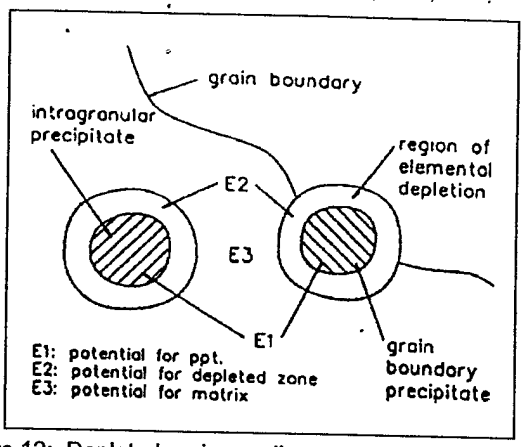

Figure 12: Depleted regions adjacent to precipitates. These regions cause an electrochemical potential difference that can promote localized corrosion at the microstructural level [1].

The formation of sufficient chromium carbide to cause sensitization can be described by the C-shaped curves on the continuous cooling diagram, as shown in Figure 13. The figure shows susceptibility to sensitization as a function of temperature, time, and carbon content. If the cooling rate is sufficiently great (curve A in Fig. 13), the cooling curve will not intersect the given C-shaped curve for chromium carbide formation and the stainless steel will not be sensitized. By decreasing the cooling rate, the cooling curve (curve B) eventually intersects the C-shape nucleation curve, indicating that sensitization may occur. At very low cooling rates, the formation of chromium carbide occurs at a higher temperature and allows for more nucleation and growth, resulting in a more extensive chromium-depleted region.

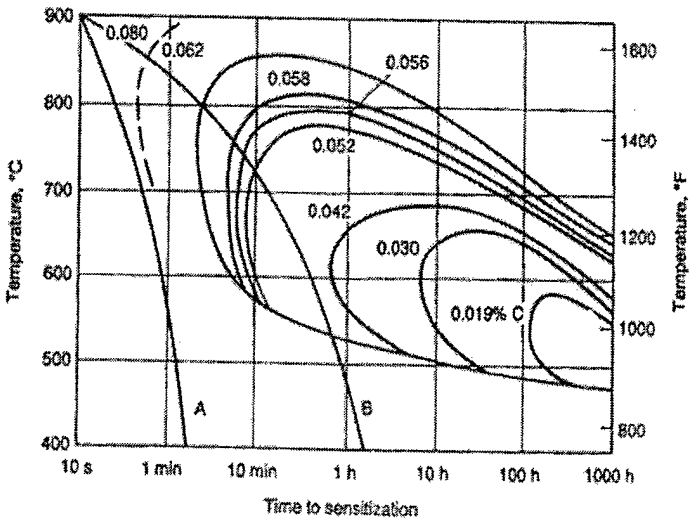

Figure 13: Time-temperature sensitization curves for Type 304 stainless steel in mixture of $CuSO_4$ and HSO_4 containing copper. Curves A and B indicate high and medium cooling rates.

The minimum time required for sensitization as a function of carbon content in a typical stainless steel alloy is depicted in Fig. 14. Because the normal welding thermal cycle is completed in approximately two minutes, for this example the carbon content must not exceed 0.07 wt. pct. to avoid sensitization. Notice that the carbide nucleation curves of Fig. 13 move down and to longer times with decreasing carbon content, making it more difficult to form carbides for a given cooling rate.

The control of stainless steel sensitization may be achieved by using:

- A post-weld high-temperature (solution) anneal and quench to redissolve the chromium at grain boundaries, and hinder chromium carbide formation on cooling
- A low-carbon grade of stainless steel (e.g. 304L or 316L) to avoid carbide formation
- A stabilized grade of stainless steel containing titanium (alloy 321) or niobium (alloy 327), which preferentially forms carbides and leaves chromium in solution. (There is the possibility of knife-line attack in stabilized grades of stainless steel.)
- A high-chromium alloy (e.g., alloy 310)

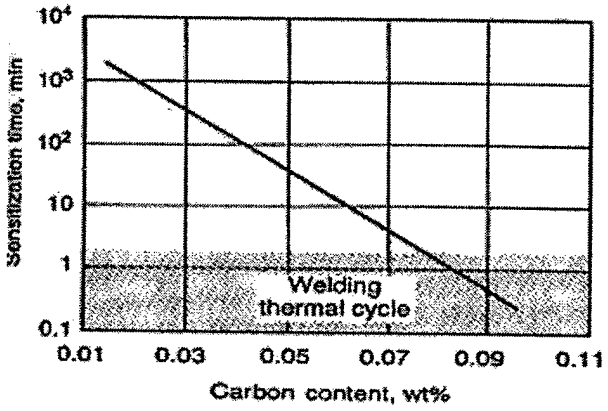

Figure 14: Minimum sensitization time from a time-temperature-sensitization diagram as a function of carbon content for a typical 300-series stainless steel alloy. [1]

6. STRESS CORROSION CRACKING

Weldments can be susceptible to stress corrosion cracking under specific environmental conditions. Stress corrosion cracking requires the proper combination of corrosive media, susceptible microstructure and tensile stress. Stress corrosion cracks have an anodic crack tip and often leave apparent corrosion products along the fracture. Cracking is often characterized by crack branching and usually has a delay time prior to crack initiation, with initiation often occurring at corrosion pits. A weld, with its various heterogeneous microstructural features, becomes an excellent candidate for stress corrosion cracking.

The thermal experience of welding is often very localized, resulting in strains that can cause distortion and residual stresses. Welds are often loaded in tension due to residual stress at a level approaching the yield strength of the base metal. Welding parameters influence the amount and distribution of residual stress because the extent of the stressed region and the amount of distortion is directly proportional to the size of the weld deposit, which in turn is directly related to the heat input. These residual stresses can be important in the generation and propagation of environmentally enhanced cracking.

It is ordinary practice to weld repair steel machinery with austenitic stainless steel consumables. This practice leaves a cathodic stainless steel weld deposit in electrical contact with the steel. In the presence of corrosive environments, hydrogen is generated at the austenitic weld metal cathode, which is capable of maintaining high hydrogen content without cracking. However, the cathodic behavior of the austenitic weld deposit may increase the susceptibility for stress-corrosion cracking in the heat-affected zone of the high-strength steel. A forty percent thermal expansion mismatch between the austenitic stainless steel and ferritic base metal, as seen in Figure 15, produces a significant residual stress field in the weldment [5]. A transverse profile of the longitudinal residual stress across an austenitic stainless steel weld deposit joining mild steel is illustrated in Figure 16 [6]. Notice that the austenitic weld deposit has a tensile longitudinal residual stress after cooling. A compressive stress occurs to the right and left of the fusion zone in the heat-affected zone resulting from the force balance relative to the tensile loaded fusion zone. Further to the outside in the heat-affected zone, a tensile residual stress zone is produced, which has values approaching the yield strength of the base metal. It is the longitudinal tensile stress that can experience transverse stress corrosion cracks in the heat-affected zone. A similar, but more localized, behavior may explain the correlation between stress-corrosion cracking susceptibility and the presence of retained austenite in high-strength steel weld deposits.

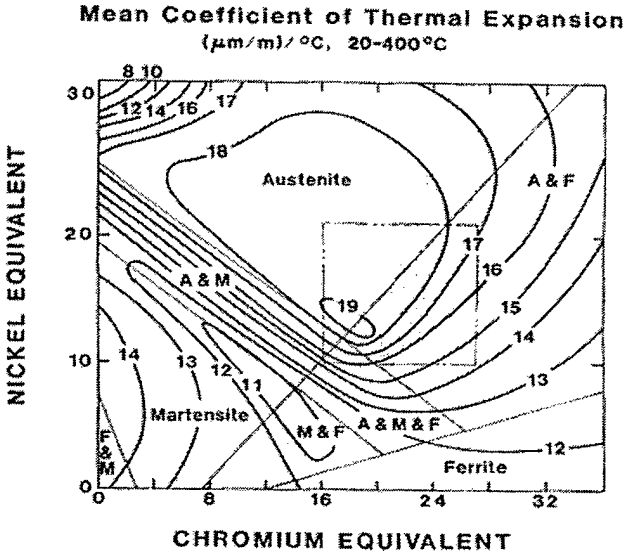

Figure 15: Mean coefficient thermal expansion (μm/m/°C, 20-400°C) plotted as isoexpansion contours on the Schaeffler constitution diagram [5].

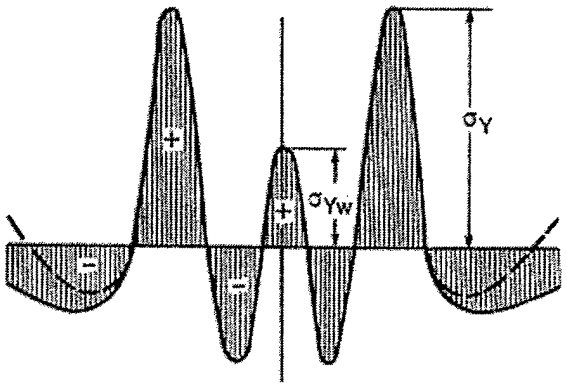

Figure 16: Weld-longitudinal residual-stresses, stress profile variants: mild steel with austenitic filler metal [6].

It is known that post-weld heat treatment can reduce the tendency for stress corrosion cracking by redistributing the localized load and reducing the magnitude of the residual tensile stress available to induce stress corrosion cracking. In a recent study on a cast austenitic stainless steel, post-solidification heat treatments were shown to also modify the local composition gradients, significantly altering the susceptibility of the solidified microstructure to stress corrosion cracking [7].

Influence of Gradients on Stress Corrosion

The influence of macro-compositional variations, resulting from solidification and modified by heat treatment, on SCC behavior has been studied [5]. Surface energy concepts were used to analyze SCC behavior. If the Griffith crack criterion is to be implemented, the strain energy of the stressed metal must be greater than the surface energy created by the incipient crack. Because SCC has been related to reductions in surface energy by the adsorption of atoms or ions from the environment, the stress intensity factor for SCC in a homogeneous material can be written as:

$$K_{ISCC} = 2(\gamma E)^{1/2} \tag{14}$$

where E is the elastic modulus and γ is the surface energy. This expression is used to relate surface tension concepts to SCC. The SCC threshold has been redefined as K_{QSCC} for cored (non-homogeneous) material [8].

The surface energy is the energy needed to create new surfaces and, like all energy considerations, requires definition with respect to a reference condition. The surface energy of a material can be defined as the energy difference between the homogeneous material prior to cracking and the same material with new surfaces resulting from cracking. In inhomogeneous systems, materials have internal compositional gradients that may alter the energy state of the material prior to fracture. Cahn and Hilliard [9] derived the interfacial tension from a thermodynamical consideration of a compositional variation in a non-uniform system. The interfacial tension is given by:

$$\gamma_1 = 2N_V \int_{Xo}^{X} G\left(\frac{dc}{dx}\right)^2 dX \tag{15}$$

where N_v is the atomic concentration per unit volume, G is the gradient energy coefficient and dc/dx is the compositional gradient. The surface energy can be modified for non-uniform systems by using the expression:

$$\gamma = \gamma_o - 2N \int_{Xo}^{X} G\left(\frac{dc}{dx}\right)^2 dX \tag{16}$$

where γ_o is the surface energy for a homogeneous system. The use of the Cahn-Hilliard expression allows for an adjustment in the initial reference energy state for the cored material, as shown in Figure 17. Notice that as the compositional gradient increases, the effective surface energy γ is reduced. A decrease in γ will reduce the stress intensity factor K_{QSCC} and make the material more susceptible to SCC. This concept suggests that in regions where the gradients are steepest, the surface energy is lowest. Correspondingly, cracks should propagate through this region.

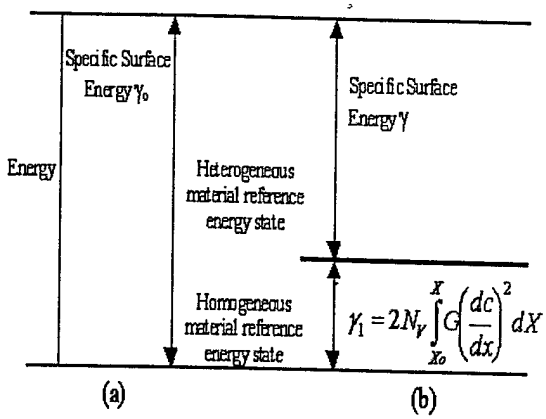

Figure 17: Energy Needed to Create Surfaces for (a) homogeneous materials and (b) heterogeneous materials [5].

If the controlling mechanism is anodic dissolution, the crack should propagate through the region of least corrosion resistance (i.e. most anodic). This region is likely to have a lower content of passivating elements, such as chromium. Figure 18 represents scanning electron microscopy microcompositional profiles across cracks in specimens. Data are shown for chromium in stainless steel casting in the as-cast condition and after annealing for either 1.5 or 19 hours. As the heat treatment time increased, the measured compositional gradients dampened. In each figure the vertical mark represents the location of the corrosion crack. The crack location is observed to cross the steepest segment of the compositional gradient for the chromium profiles.

These results represent preliminary evidence that stress corrosion cracks follow the regions in which the compositional gradients are the steepest as predicted by :

$$K_{QSCC} = 2\left\{E\left[\gamma_o - 2N \int_{Xo}^{X} G\left(\frac{dc}{dx}\right)^2 dx\right]\right\}^{1/2} \tag{17}$$

These results give us a better understanding of the role of post-weld heat treatment in reducing SCC susceptibility. It has been commonly believed that post-weld heat treatment influences the susceptibility to SCC by redistributing the load and thus reducing the local stress. This work suggests that post-weld heat treatment also influences the electrochemical and interfacial promotion of SCC by dampening the compositional variation common to solidified structures.

These results would suggest that alloy systems that exhibit large degrees of microsegregation during solidification may be more susceptible to SCC. The relationship between the partition ratios and susceptibility to SCC needs to be further investigated.

7. HYDROGEN ASSISTED CRACKING

Traditionally Hydrogen Assisted Cracking (HAC) is associated with the heat affected zone (HAZ) location of carbon manganese steel welds. The carbon level in the HAZ is fixed at the base material, while low carbon filler metals decrease the occurrence of HAC in the weld metal. With the carbon level of newer high strength steels being much lower than in the conventional steels, the occurrence of HAC in the weld metal is now becoming an issue.

The primary focus in managing weld metal HAC has been on the development of welding consumables and practice. Wong has proposed a crack prediction model based on the WIC and modified cruciform tests [10]. This model, which uses the Yurioka method to predict HAZ pre-heat, was adapted for weld metal cracking problems [11].

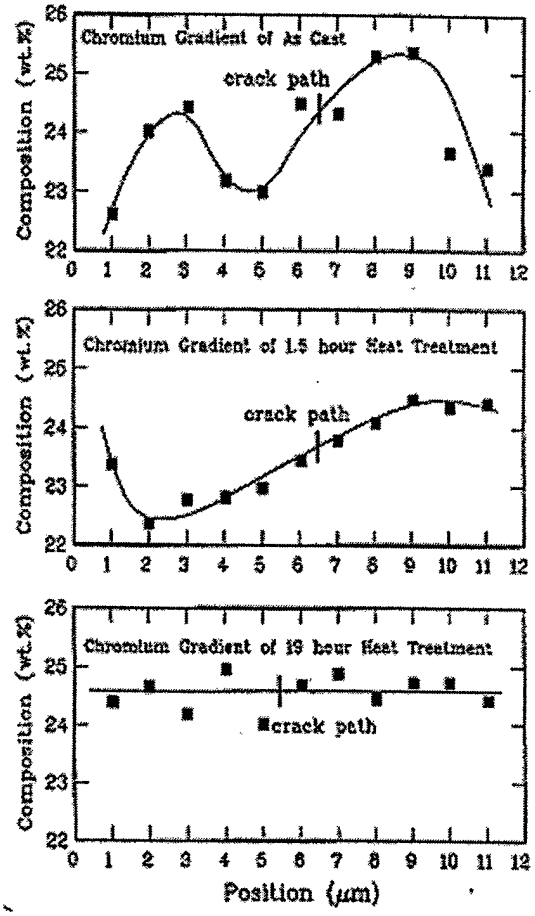

Figure 18: Chromium micro-compositional scans across stress corrosion cracks of CK-20 stainless steel castings in three different heat treat conditions on unetched surfaces. Vertical line is the position of the stress corrosion crack [7].

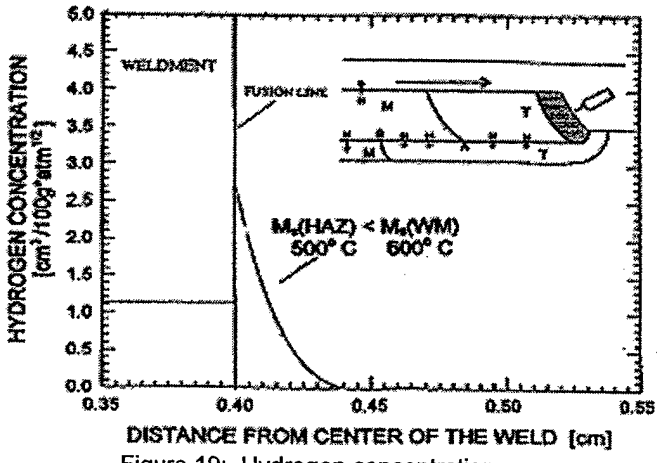

Figure 19: Hydrogen concentration as a function of distance from the weld center with the HAZ M_S temperature less than the weld metal M_S temperature.

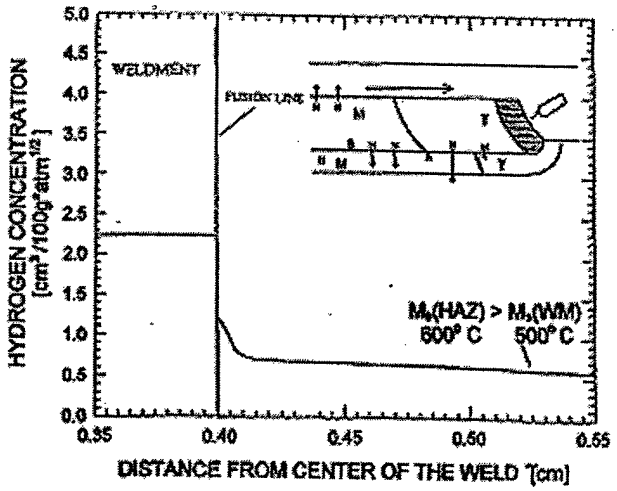

Figure 20: Hydrogen concentration as a function of distance from the weld center with the HAZ M_S temperature greater than the weld metal M_S temperature.

The transformation temperature of the weld metal can be either higher or lower than that of the base material, depending on the filler and base metal compositions. Wang *et al.* [12] report that the location of hydrogen cracks depends to a great extent on the relative martensite start temperatures of the two zones. If the *Ms* of the weld metal is higher than that of the heat affected zone, hydrogen accumulates in the coarse grained HAZ region. The austenite acts as a barrier to hydrogen movement into the heat-affected zone allowing for the hydrogen accumulation in the boundary area and causing the HAC problem at this location (Figure 19). However, if the M_S of the weld metal is lower than that of the heat affected zone, there is less hydrogen accumulation in the sensitive boundary region and HAC is more likely in the weld metal (Figure 20). Wang *et al.* proposed an index based on the weld metal/HAZ difference in martensite start temperature [12]. Expressions for calculating M_S in both base metal and weld metal are available [13]. The fracture occurs in either the weld metal or HAZ, depending upon which one first reaches the critical combination of sensitive microstructure, residual stress level and hydrogen. This ability to correlate HAC to the martensitic start temperature of the weld deposit is illustrated in Figure 21.

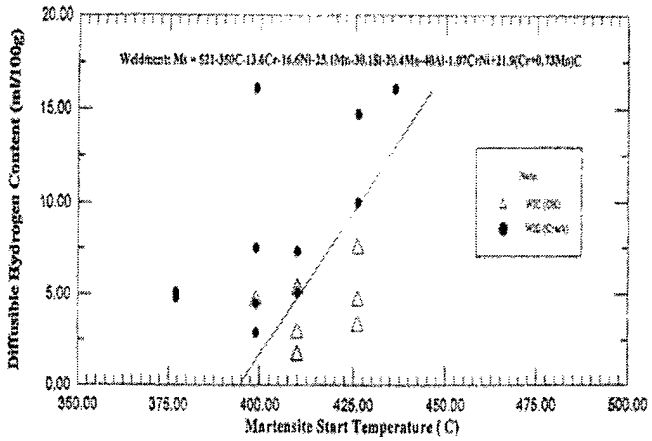

Figure 21: Illustration of hydrogen cracking/uncracking zones by hydrogen content and martensite start temperature [12].

With the use of higher strength steels, the weld hydrogen content needs to be maintained at even lower content levels and for these new steels the issue is not just the hydrogen content but also hydrogen distribution relative to the weld deposit. New methods to reduce the diffusible hydrogen content include weld metal hydrogen gettering and fluoride additions.

Effective control of weld diffusible hydrogen content in higher strength steel weld deposits has been achieved with the use of irreversible hydrogen traps. The benefit of weld metal yttrium as an irreversible hydrogen trap was reported by Maroef *et al.* [14] to decrease the diffusible hydrogen content in the weld metal to appreciable levels around 1 to 2 ml of hydrogen per 100 g weld deposit (0.89 to 1.8 wt. ppm of hydrogen). The weld metal diffusible hydrogen content is affected by variations in welding parameters. The spray mode, with its fine metal droplets, has the ability to react the yttrium with oxygen, resulting in a large concentration of hydrogen trapping inclusions in the weld metal.

The use of selected fluoride additions to welding consumables to promote a plasma chemistry that reduces the weld pool hydrogen content has been demonstrated by Pokhodnya [15] and Matsunawa *et al* [16]. Various fluoride additions have been added to the electrode covering, resulting in welds in which the diffusible hydrogen contents have been dropped from 5 ml/100 gram of iron to 1.5 ml/100 gram of iron, a significant reduction. Reductions in diffusible hydrogen levels were measured with additions of $AlSiF_2$, KF, MnF_3 and K_3AlF_6.

8. MICROBIOLOGICALLY INFLUENCED CORROSION

Microbiologically Influenced Corrosion (MIC) is a phenomenon in which microorganisms play an important role in the corrosion of metals. MIC can initiate or accelerate the corrosion process. For example, water and some organic media may contain certain microorganisms that can produce a bio-film when exposed to a metal surface. The resulting non-uniform coverage may lead to a concentration cell and eventually initiate corrosion. Additionally, the microorganisms metabolic process can produce a localized acidic environment that changes the corrosion behavior of the exposed metal by altering anodic and cathodic reactions, destroying protective films, or creating corrosive deposits [17]. Both aerobic and anaerobic bacteria have been identified as contributors to this type of damage. These bacteria usually convert sulfur from the metal into sulfuric acid. Often pits, that are formed by MIC, have inside edges that are terraced and have the appearance of a micro open-pit mine.

In austenitic stainless steel weldments, the effects of MIC are usually observed as pitting on or adjacent to welds [18, 19]. MIC attacks either γ or α phases even if the water has a crucially low chloride content. Pits are found in regions of the heat-affected zone, at the fusion line, and in the base metal near the weld. There is also evidence of MIC occurring along with stress corrosion cracking in weldments of austenitic stainless steel. Welding design and plant operations can minimize MIC attack by preventing an adequate environment for microorganisms.

9. CONCLUSIONS

Fundamental concepts were introduced to give insight into the specific corrosion behaviors associated with the non-uniform nature associated with weldments.

10. ACKNOWLEDGEMENTS

The authors acknowledge and appreciate the NSF fellowship support and ARO research support.

11. REFERENCES

1. ASM Handbook. (1993). Welding, Brazing, and Soldering: Corrosion of Weldments. Vol. 6 (10), pp 1065-1069.
2. Mishra, B., Olson, D.L., and Lensing, C. (1998). The Influence of Weld Microstructural Features on Corrosion Behavior, PRICM 3, TMS Warrendale, PA., pp 2303-2308.
3. Enerhaug, J., Grong, Ø., Steinsmo, U.M., (2001) "Factors Affecting Initiation of Pitting Corrosion in Super Martensitic Stainless Steels", Science and Technology Welding and Joining. Vol 6 (5), pp 334-335.
4. Porter, D.A., and Easterling, K.E., (1992) "Phase Transformations in Metals and Alloys" pp 314-317. Chapman and Hill, N.Y., N.Y.
5. J.W. Elmer, D.L. Olson, and D.K. Matlock, (1982), "The Thermal Expansion Characteristics of Stainless Steel Weld Metal," Welding Journal, Vol_(9), pp293s-301s.
6. D. Radaj, (1992) "Heat Effects of Welding," Springer-Verlag, Berlin, pp 201.
7. Berry, Jr. G.J., Olson, D.L., and Matlock, D.K. (1991) "Influence of Microcompositional Gradients on Stress Corrosion Crack Propagation", Materials Sci. and Engr. A148, pp 1-6.
8. Gooch, T.G., (1974), "Stress Corrosion Cracking of Welded Joints in High Strength Steels Weld", Vol. 53 (7), pp 2877-2982.
9. Cahn, J.W. and Hilliard, J.E., (1958), "Free Energy of a Non-Uniform System. I Interfacial Free Energy", J. Chem. Phys. Vol 28 (2), pp 258-267.
10. Wong, R.J. (1996), "Hydrogen Induced Cracking in High Strength Steel Weldments," Proc. Intl. Conf. On Advances in Welding Technology, EWI, pp 347-357.
11. Yurioka, N., Suzuki, H., Ohshita, S., and Saito, S. (1983), "Determination of Necessary Preheating Temperature in Steel Welding", Weld. J. Vol 62 (6), pp 147s-153s.
12. Wang, W.W., Wong, R., Liu, S., and Olson, D.L. (1996), "Use of Martensite Start Temperature for Hydrogen Control" in "Welding and Weld Automation in Shipbuilding," TMS, Warrendale, PA, pp 17-31.
13. J.A. Self, B.F. Carpenter, D.L. Olson, and D.K. Matlock, (1987), "Phase Transformations and Alloy Stability" in "Alternate Alloying for Environmental Resistance," TMS, Warrendale, PA, pp 37-45.
14. Maroef, I.S., Park, Y.D., Lensing, C.A., and Olson, D.L. (2000) "Hydrogen Trapping of High Strength Steel Weld Metal", Journal of Advanced and Specialty Materials, ASM Materials Park, OH. pp 284-291.
15. Pokhodnya, I.K. (1996), "Hydrogen Behavior in Welding Joints", P.O. Paton Electric Welding Institute, Mat. Acad. Sci. of Ukraine, Kiev.
16. Matsunawa, M. and Liu, S. (2000), "Hydrogen Control in Steel Weld Metal by Means of Fluoride Additions in Welding Flux", Weld. J. Vol. 79 (10), pp 295s-303s.
17. S.C. Dexter. (1987), Localized Biological Corrosion, Metals Handbook, Vol. 13. 9th ed., ASM. Materials Park, Ohio, pp 114-120.

18. G.J. Licina, (1988) "Sourcebook of Microbiologically Influenced Corrosion in Nuclear Power Plants", NP5580, Electric Power Research Institute, Palo Alto, CA.
19. S. W. Borenstein, (1988) "Microbiologically Influenced Corrosion Failures of Austenitic Stainless Steel Welds," Paper 78, Corrosion '88, NACE, Houston, TX.